Proceedings of the Canadian Society for Mechanical Engineering International Congress
32nd Annual Conference of the Computational Fluid Dynamics Society of Canada
Canadian Society of Rheology Symposium
CSME/CFDSC/CSR 2025
May 25–28, 2025, Montréal, Québec, Canada

NUMBER

Supercritical CO_2 heat transfer enhancement in large diameter horizontal tubes by internal fins

Seyed Mojtaba Hosseinnia*, Antoine Metsue, Leyla Amiri, Sébastien Poncet

Mechanical engineering department, Université de Sherbrooke, Sherbrooke, Canada
*seyed.mojtaba.hosseinnia@usherbrooke.ca

February 11, 2025

***Abstract*—**CO_2 is a natural refrigerant with low global warming potential, widely employed in refrigeration, heat pumps, and power generation cycles. The thermophysical properties of supercritical CO_2 (s-CO_2) near the pseudo-critical point exhibit significant variation with temperature. In horizontally heated tubes, buoyancy force within the gravitational field causes the hotter, gas-like s-CO_2 to accumulate near the top, while the cooler, liquid-like s-CO_2 remains concentrated in the center and lower regions. This non-uniform temperature distribution reduces heat transfer coefficients along both the axial and circumferential directions, particularly at the top of the tube. To mitigate this issue, this study investigates the incorporation of eight thin internal fins within a horizontally oriented, large-diameter steel tube to enhance heat transfer performance in a high buoyancy force (i.e., Richardson number > 0.1). A numerical investigation is performed for a 3D horizontal tube with an inner diameter of $22.14\,mm$, subjected to a high heat flux boundary condition. The numerical results are validated against experimental data for a smooth horizontal tube, demonstrating good agreement with a maximum temperature error of less than 5%. The fins facilitate heat transfer towards the cooler regions of the s-CO_2, significantly modify flow circulation, and promote mixing, thereby improving heat transfer efficiency. The results reveal that the internally finned tube achieves the same heat transfer rate using 5.7% less tube solid mass and reduces the maximum temperature at the end of the heated section by 50.8%. These findings underscore the potential of internally finned horizontal tubes to enable more cost-effective and efficient heat exchanger designs.

***Keywords-component*—supercritical CO_2; horizontal tube; internal fins; numerical modeling**

I. INTRODUCTION

Applications of CO_2 (R744) in different energy systems including but not limited to high temperature heat pumps [7], refrigeration systems [20], and power generation cycles [9] are increasing. Due to the global warming potential (GWP) and other environmental issues of fluorocarbon-based refrigerants, CO_2 is one of their best replacements, which has a low GWP value; it is non-toxic, non-flammable, and relatively cost-effective [12]. However, there is one main concern in the CO_2 application as a working fluid: high working pressure. The high operating pressure results in high equipment cost and certification issues.

The critical temperature and pressure of CO_2 are $T_{crt} = 31\,^oC$ and $P_{crt} = 7.38\,MPa$, respectively. In other words, at pressures above P_{crt} and at temperatures above T_{crt}, it behaves like a gas, while below T_{crt}, CO_2 behaves like a liquid. Therefore, when it undergoes a heating or cooling process at operating conditions close to the critical or pseudo-critical point, strong variations in thermophysical properties start playing a role, especially in the Earth's gravitational field. Strong buoyancy forces the hot part to move upward alongside the tube wall, then this heated part stays there, creating a relatively high temperature zone. This results in a drop in the heat transfer coefficient at the top of the tube in comparison to the sides and the bottom of the tube. Low CO_2 mass flowrate, high surface heat flux, and large diameters of horizontal tubes in bundles make the temperature difference between top and the bottom higher. The temperature difference between the bulk fluid and the top part of the horizontal tube can be as high as 100°C in some cases, depending on the wall heat flux value [1]. This phenomenon is named heat transfer deterioration in the literature [18].

In general, different methods and techniques have been applied to enhance the heat transfer in horizontal tubes including adding internal fins [10], [13], helical wire inserts [8], spacers [5], and grooves [19]. For example, Pai and Yeh [13] inves-

Identify applicable sponsor/s here. (*sponsors)*

tigated the addition of trapezoidal internal fins in a double-tube water-to-water heat exchanger in laminar flow. Rustum and Soliman [14] studied the addition of rectangular internal fins in laminar mixed convection in horizontal tubes. Wang et al. [17] explored adding new type left–right symmetric internal fins into horizontal tubes where flue gas flows inside the tubes. A 4 to 8 times increase in heat transfer coefficient is reported compared to the smooth no-fin tube. In all of the mentioned studies, the thermophysical properties are kept constant. Recently, Shome [15] studied the presence of internal rectangular fins in a vertical tube where helium is heated. By increasing the number of fins from 8 to 24, large reduction in the turbulent kinetic energy was detected. Also the flow velocity in inter-fin regions reduced meaningfully. This process is named laminarization. It should be noted that this study did not include the solid body of the fins in the computational domain.

Enhancing heat transfer rate of s-CO_2 at a given operating condition by adding internal fins is the objective of this study. Internal fins have not been applied to large horizontal tubes with s-CO_2 as the working fluid. Thus, in this study, internal fins are introduced into the s-CO_2 flows at a constant mass flow rate of 0.146 kg.s^{-1} and high average wall heat flux of 26.9 kW.m^{-2}. The idea here is to conduct heat from the top hot part towards the center and down region of the tube and alter the flow circulation by introducing internal fins. It should be noted that finding the optimal fin profile is not a trivial task. Therefore, the optimal profile obtained for pin fins in [3] is used in this study with some modifications and scaling.

II. Numerical details

A. Computational domain and mesh design

The computational domain consists of a horizontal tube with an outer diameter of $D = 25.4mm$ (1 inch) and a thickness of $1.63mm$. The length of the unheated (i.e. adiabatic) and heated sections is $55D$ and $110D$, respectively. It should be noted that these dimensions are set in accordance with the available experimental data [1]. Figure 1 illustrates the cross-section view of the finned tube and the mesh design close view of the tip of the bottom fin. All cells are hexahedral, and all fins are identical, with $6\,mm$ height and $2\,mm$ as the base thickness. The fins are distributed in a constant center-to-center 45 degree tangential arrangement. Due to the complicated curvature of the fins' body, the grid size needs to be refined near the curvatures. Also, the first cell height is set to $0.0005\,mm$ with a growth rate of 1.08 to have a y^+ value at the fluid/solid wall less than 0.1, as suggested in [4]. Taking advantage of the symmetry with respect to the y-z plane, only half of the tube is modeled. A grid independence study was conducted, achieving convergence with approximately 70 million cells in the computational domain. The cell thickness in the $-z$ direction is set to $800\,\mu$m.

B. Governing equations and turbulence model

The governing equations consist of continuity, momentum, energy, and turbulence equations. The coupled algorithm is used for velocity-pressure coupling. Second-order discretization is used for all equations. The k-ω shear stress transport (SST) is selected as turbulence closure in the ANSYS Fluent finite volume solver [2]. As the constant turbulent Prandtl number cannot accurately predict the temperature distribution in the computational domain, a variable one is used in this study, originally proposed by Tang et al. [16]:

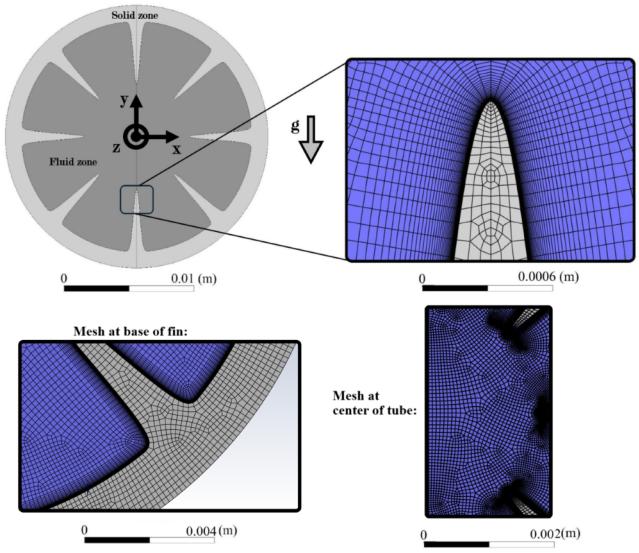

Figure. 1. Internally finned tube cross-section view and the grid distribution near the tip of the bottom fin, the base of the fin, and the center of the tube

$$\mathrm{Pr}_t = \begin{cases} 1.0 & \frac{\mu_t}{\mu} < 0.2 \\ 0.85 + \frac{\mathrm{Pr}}{A} & 0.2 \leq \frac{\mu_t}{\mu} \leq 10 \\ 0.85 & 10 < \frac{\mu_t}{\mu} \end{cases} \quad (1)$$

where Pr is the Prandtl number, μ and μ_t are the molecular and turbulence viscosities, respectively. A is a tuning parameter which is set to 17, suggested in [4]. More details can be found in [4], [16].

C. Boundary conditions

To be consistent with the experimental study, which is used here for validating the model, a constant volumetric heat source is applied in the solid part (not the fins) of the computational domain, based on an average heat flux value of $26.9\,kW.m^{-2}$. The mass flow inlet boundary condition equal to $0.146\,kg.s^{-1}$ is applied at the inlet, and the zero normal gradient (i.e., outflow) boundary is considered for the outlet. The heat loss to the ambient is neglected. Moreover, the variations in the thermophysical properties of s-CO_2, specifically near the pseudo-critical point, are included by hooking property tables via user-defined functions to the ANSYS Fluent solver. Details of the table algorithm for s-CO_2 properties can be found in [11]. Figure 2 illustrates the thermophysical properties of s-CO_2 in the considered operating pressure of $7.586\,MPa$ in a wide range of possible operating temperatures. The corresponding pseudo-critical temperature is $32.22\,^oC$. As can be seen from Figure 2, the density (ρ) of the s-CO_2 drops sharply

by approaching towards the pseudo-critical temperature from a liquid-like region. However, specific heat capacity (c_p) illustrates a step-function like jump near the pseudo-critical temperature from $2.94\,kJ.kg^{-1}.K^{-1}$ to $123.9\,kJ.kg^{-1}.K^{-1}$. The variations of thermal conductivity (κ) and viscosity (μ) are moderate in comparison to the density and c_p.

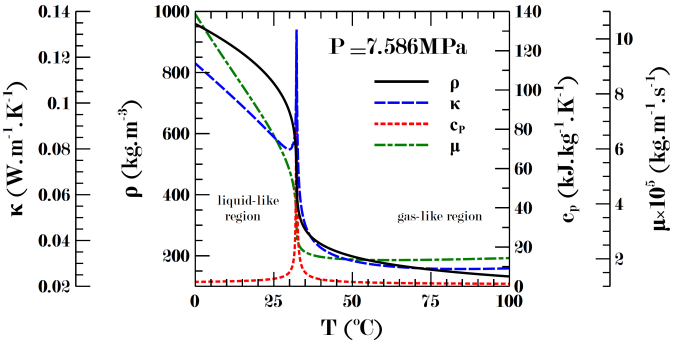

Figure. 2. Variations in thermophysical properties of s-CO_2 at the studied operating condition

It is worth noting that at the same operating pressure, at operating temperatures below the pseudo-critical one, s-CO_2 properties will be like a liquid. Thus, it is called liquid-like s-CO_2, while at the temperatures above the pseudo-critical, the s-CO_2 acts like a gas; therefore, it is named gas-like s-CO_2. Additionally, the density, thermal conductivity, and specific heat capacity of the steel tube are set as $8030\,kg.m^{-3}$, $16.7\,W.m^{-2}.K^{-1}$, and $502.48\,J.kg^{-1}.K^{-1}$, respectively. Further, the gravitational acceleration is applied downward with a constant value of $9.806\,m.s^{-2}$. The simulations are performed with High Performance Computing on Digital Research Alliance of Canada (Narval cluster) with 64 CPUs and 320 Gb of RAM. The convergence criteria for continuity, momentum, energy, and turbulence equations are set to 10^{-5}, 10^{-8}, 10^{-9}, and 10^{-7}, respectively.

III. Results and Discussion

In this section, first, the accuracy of the performed simulation is verified against available experimental data. Then, the hydrodynamics and heat transfer of the smooth and finned tube will be discussed.

A. Validation

Figure 2 illustrates the axial temperature variations, obtained from the CFD simulation against the experimental data [1] for a horizontal smooth tube at the same operating conditions. The maximum error between the CFD simulation and the experimental data is less than 4.1% , which can be interpreted as a good agreement.

By evaluating the accuracy of the CFD modeling, the hydrodynamic and the temperature distribution details can be discussed in the following sections.

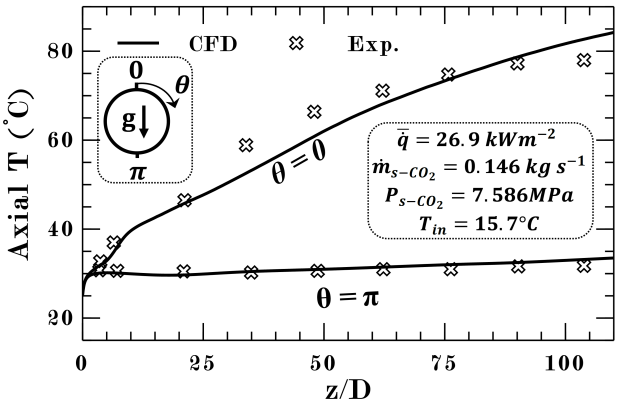

Figure. 3. Axial temperature variations at the top (θ = 0) and the bottom (θ = π) of the smooth horizontal tube in the heated area (Exp. data from [1])

B. Fin impacts on the flow hydrodynamic

Figure 4 illustrates the fully developed velocity profiles for both smooth and the finned tubes at the beginning and the end of the heated section. As expected, the maximum velocity at the center of the finned tube is 39% higher in comparison to the smooth tube. This can be partly attributed to the cross section area of the fluid passage as it is reduced by 8.6% (the hydraulic diameter is 43% smaller than that of the smooth tube).

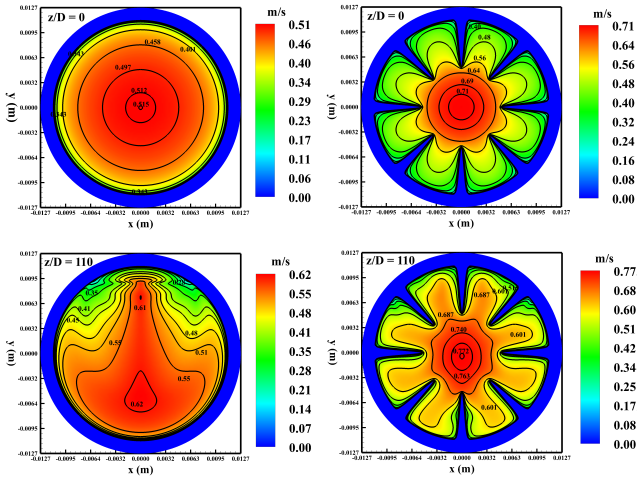

Figure. 4. Velocity profiles of s-CO_2 at the beginning (z/D =0) and the end (z/D =110) of the heated section in both smooth and finned tubes

Further, the no-slip condition on the solid walls, in combination with the buoyancy effect of the hot wall with respect to the colder s-CO_2 at the bulk of the tube, generates some circulation (i.e., buoyancy currents) in the fluid zone. Figure 5 depicts these circulations at the cross-section of both smooth and finned tubes at the end of the heated section. The strength of the circulations can be estimated via 2D velocity magnitude, i.e. $\sqrt{(V_x)^2 + (V_y)^2}$. In smooth tube, the buoyancy current forms one large and strong circulation in the main fluid

body and two weak ones at the top of the tube, while the finned tube presents several circulations: one weak close to the center of the tube, two circulations in the bottom bay (one close to its right corner and the other close to its center), two weak circulations in the top bay, and one circulation in each side bay. Overall, the maximum 2D velocity magnitudes are $0.046\,m.s^{-1}$ and $0.033\,m.s^{-1}$ for the smooth and the finned tubes. Although the 2D velocity magnitude is lower in the finned tube, the higher effective circulations due to the presence of the fins result in a more homogeneous velocity in the cross-section of the finned tube. Additionally, the presence of the fins weakens the buoyancy currents, which can be interpreted as the laminarization of the turbulent flow, as shown by Shome in [15]. It should also be mentioned that adding to the fin numbers will impede the buoyancy currents even more and the laminarization of the flow will be enhanced in cost of higher pressure drop.

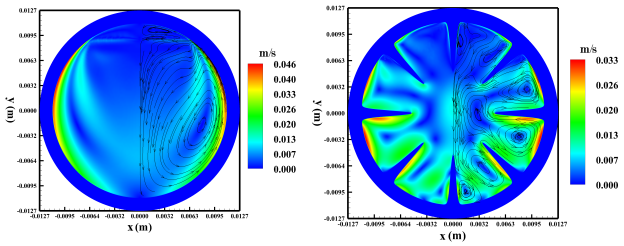

Figure. 5. 2D velocity contours and circulation streamlines in z/d =110; left: smooth tube, right: finned tube

C. Heat transfer enhancement by fins

Figure 6 depicts the temperature contours of s-CO_2 and the tube solid part at the end of the heated section for both smooth and finned tubes. Generally, due to the buoyancy effect, the colder fluid moves to the bottom of the tube, while the warmer one moves upward. This general behavior is observed in both smooth and finned tubes. As seen in the hydrodynamic section, the motion of fluid due to buoyancy results in local flow circulations and augmentations of the hot fluid at the top part of the tube, especially in the smooth tube. As the hot fluid at the top will not get mixed with the center part, its temperature tends to increase even to the higher temperatures. By adding fins, the maximum temperature of s-CO_2 is significantly reduced: 45^oC in comparison to 84^oC for the smooth tube. This observation is attributed to the role of the fins in forming local circulation inside the confined volume between fins instead of having one large circulation, as seen in the smooth tube. Also, the extended solid surface conducts more heat toward the central part of the main fluid flow, increasing the uniformity of the temperature field.

In contrary to the lower maximum temperature in the finned tube, the bulk temperature of the s-CO_2 inside the finned tube is higher than the bulk temperature in the smooth tube. This is the main contribution of the extended surface by the fins. However, this superior heating characteristic has not gained freely. It comes with two penalties: a higher pressure drop and

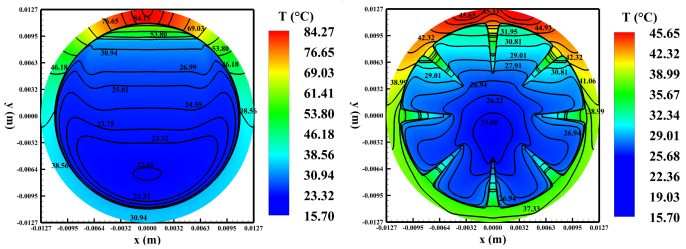

Figure. 6. Temperature contours at z/D =110; left: smooth tube, right: finned tube

a higher weight of the tube per meter. The latter is directly related to the cost of the tube. Figure 7 illustrates the bulk temperature and pressure drop along the axis of the tube for both smooth and finned tubes. As the mass flowrate is kept constant for both studied cases, higher bulk temperature means shorter tube length for having the same heating duty. Therefore, the overall required fabrication material will be lower when using the finned tube in a heat exchanger. As an example, the heat transfer rate can be computed as:

$$\dot{Q} = \dot{m}_{s-CO_2}[h_{out}(T_{out}, P_{out}) - h_{in}(T_{in}, P_{in})] \qquad (2)$$

where $\dot{Q}$ is the heat transfer rate (in kW), h is the enthalpy of the s-CO_2 at the end and beginning of the heated section at the corresponding bulk temperature and pressure. For the smooth tube and the heated length of $2.44\,m$, the total heat transfer rate is $4.3\,kW$. The same heat transfer rate can be achieved with the finned tube with a heated length of $1.808\,m$. At this length, the finned tube mass is 5.7% less than that of the smooth tube. In other words, although the mass per meter of the finned tube is higher in comparison to the smooth tube, its heat transfer superiority makes the required tube length shorter for the same heating load; therefore, the total mass of the heat exchanger fabricated by the finned tube goes down, so does its cost. Regarding the imposed pressure drop, the main drawback of adding internal fins is higher pressure drop. Here, by adding 8 fins, the pressure drop is increased by a factor of 2.8. In other words, ΔP increases from $141\,Pa$ to $393.8\,Pa$ by adding the fins to the smooth tube at current dimensions and arrangement.

Moreover, Figure 8 depicts the local wall temperature and Richardson number (Ri) for both smooth and finned horizontal tubes at the end of the heated section. Ri is an indication of the strength of the buoyancy to the shear forces in the mixed convection heat transfer. It is defined as:

$$Ri = \frac{Gr}{Re^2} \qquad (3)$$

where Gr is the Grashof number:

$$Gr = \frac{\rho_b - \rho_w}{\rho_b} \cdot \frac{gD_h^3}{\nu_b^2} \qquad (4)$$

ρ_b and ν_b are the bulk density and kinematic viscosity of s-CO_2 in the given cross-section ($\nu_b = \rho_b/\mu_b$), ρ_w is the density

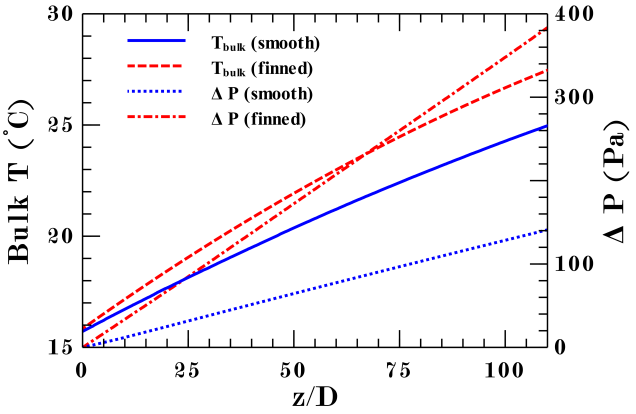

Figure. 7. Bulk temperature and pressure drop variations along the axis of the smooth and finned tubes

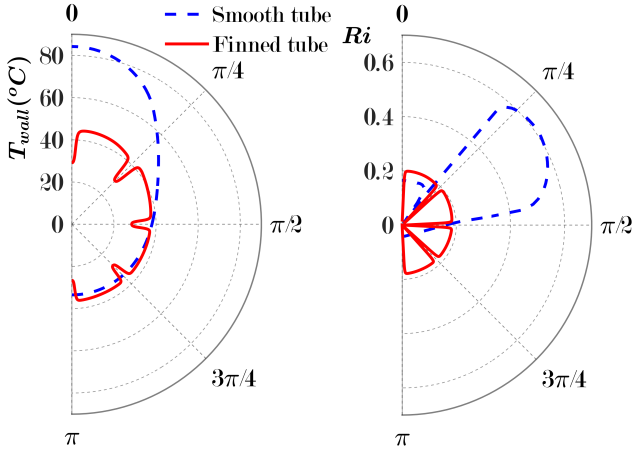

Figure. 8. Local tangential wall temperature and Richardson number in both smooth and finned tubes

of s-CO_2 at the wall, D_h is the hydraulic diameter of the tube, and g is the gravitational acceleration. it should be noted that the wall temperature is a local value, it changes at different location on the internal wall of the tube, in both smooth and finned tube.

The Reynolds number is computed via [6]:

$$Re = \frac{\dot{m} D_h}{\mu_b A_c} \tag{5}$$

$\dot{m}$ is the mass flowrate, μ_b is the bulk viscosity of the s-CO_2 at the given cross-section, and A_c is the cross-section area, that is $175.9\,mm^2$ in the finned tube case. The local tangential temperature varies from 0 to π at the wall surface, so does the density of s-CO_2. Thus, the variations in the thermophysical properties will be reflected in the Ri number. In both smooth and finned tubes, Ri ranges between 0.1 to 1, which indicates that the effect of the buoyancy cannot be neglected in this problem. It should be emphasized that the finned tube has a lower local Ri number in comparison to the smooth tube due mainly to the lower density difference between the fluid bulk and the density near the wall.

Additionally, the local heat transfer coefficients (HTC) can be computed by Eq. (6):

$$HTC = \frac{\dot{q}_w}{|T_w - T_b|} \tag{6}$$

Local HTCs are shown in Figure 9 and Figure 10 for axial values in the heated section and tangential values at the end of the heated section, respectively. The HTC deterioration can be seen in the top part of the smooth heated tube while the bottom part has a reasonably high HTC. The top and bottom axial lines in the smooth tube are corresponding to the maximum and minimum temperatures of the tube. Nonetheless, the maximum temperature occurs at the top-left corner of the top bay (i.e. $\theta = 5.2^oC$) in the finned tube. The minimum temperature happens to be at the tip of the fin located at $\theta = \pi$. Therefore, the axial lines passing through these two points are selected for plotting the local axial HTCs. A peak value can be seen in the HTC corresponding to the minimum wall temperature in the finned tube as the bulk and wall temperatures share the same value. It should be noted that the HTC approaches infinity as the wall heat flux is divided by zero. Further, the change in the sign of $T_w - T_b$ at the tip of the bottom fin indicates that its height is unnecessarily high and should be reduced in a new design. Nevertheless, the height of the fins also affects the hydrodynamics of the flow, the pressure drop, and through these, the heat transfer rate will be influenced. In other words, the geometry of the fins should be carefully selected for the best results: maximizing the heat transfer while minimizing the pressure drop.

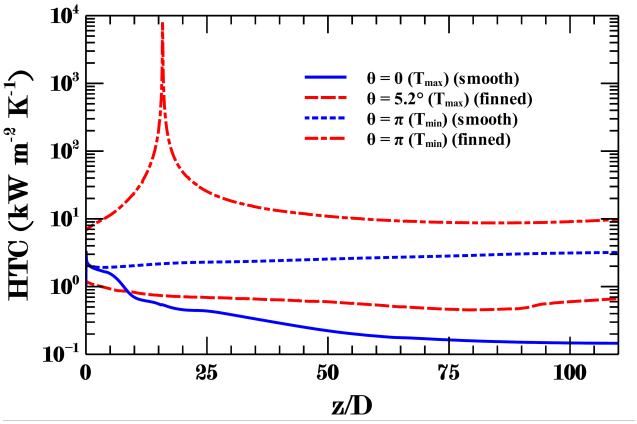

Figure. 9. Local HTC at the hottest and coldest wall points along the axis of the smooth and finned tubes

The tangential distribution of the heat flux at the s-CO_2-tube wall and the HTC in Figure 10 depicts several sharp fluctuations in wall regions near the fins. This is mainly due to the variations in the local heat flux, the wall temperature, and the corresponding fluid temperature near the wall. Local heat flux on the inner wall of the tube reduces as the local wall temperature goes up. It should be noted that the heat flux at the inner wall of the tube deviates from the average heat flux

of $26.9\,kW.m^{-2}$. It shows that applying boundary conditions in the numerical analysis is very important.

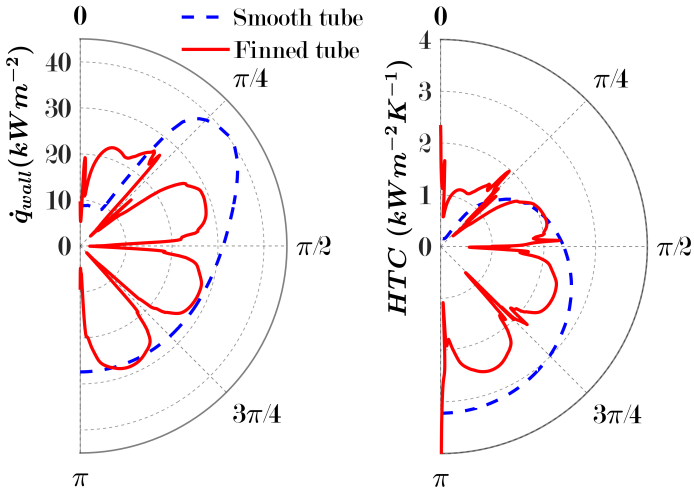

Figure. 10. Local tangential variations of HTC at the end of the heated section for both smooth and finned tubes

IV. Conclusion

Adding internal fins to large-diameter horizontal tubes with an inner diameter of $22.14\,mm$, where turbulent s-CO_2 flows, significantly enhances the heat transfer rate, around 35%, in comparison to the smooth tube for a mass flowrate of $0.146\,kg.s^{-1}$, operating pressure of $7.586\,MPa$, inlet temperature of $15.7\,^oC$, and high average heat flux of $26.9\,kW.m^{-2}$. A detailed analysis of the flow hydrodynamics and temperature profiles reveals that the large 2D flow circulation in a smooth tube is replaced with 5 smaller circulations inside each bay between the 8 fins. Also, a notable reduction in the maximum temperature at the top of the horizontal tube, accompanied by an increase in the heat transfer rate is observed. Local axial HTC values illustrates that the height of the bottom fins in current design is more than what is required as the tip temperature of this fin is less than the bulk fluid temperature after $z/D = 16.5$. The local Ri number clearly indicates that the buoyancy currents are impeded by implementing the fins. For instance, the maximum Ri number is 0.6 at the end of the heated section in the smooth tube, compared to 0.21 in the finned tube. Further, for the same heating duty, the finned tube requires 5.6% less material, although it results in a 2.6-fold increase in pressure drop. The reduced mass of the steel finned tube lowers the overall cost of the heat exchanger designed for the same heating duty. The number, length, and distribution of fins can be optimized to minimize the pressure drop while maintaining or even improving the heat transfer rate. This optimization will be addressed in future studies.

Acknowledgment

The authors acknowledge the support of the NSERC chair on industrial energy efficiency established in 2019 at Université de Sherbrooke and funded by Hydro-Québec (laboratoire des technologies de l'énergie), Natural Resources Canada (CanmetEnergy-Varennes) and Copeland Canada Inc. All calculations have done using the HPC facilities of the Digital Research Alliance of Canada.

References

[1] G. Adebiyi and W. Hall. Experimental investigation of heat transfer to supercritical pressure carbon dioxide in a horizontal pipe. *International Journal of Heat and Mass Transfer*, 19(7):715–720, 1976.

[2] ANSYS Inc. *Ansys Fluent Theory Guide*, 2023. V2023R1.

[3] B. P. Belinskiy, J. W. Hiestand, and L. Weerasena. Optimal design of a fin in steady-state. *Applied Mathematical Modelling*, 77:1188–1200, 2020.

[4] J. Hou, Y. Zhou, Y. Yuan, and S. Huang. Numerical study on flow structure and heat transfer of supercritical CO_2 in tubes with different inclination angles. *Progress in Nuclear Energy*, 168:105028, 2024.

[5] Z. Hu and H. Gu. Heat transfer of supercritical water in annuli with spacers. *International Journal of Heat and Mass Transfer*, 120:411–421, 2018.

[6] W. M. Kays and Crawford. *Convective heat and mass transfer*, volume 3. McGraw-Hill New York, 1993.

[7] L. Kong, T. G. Walmsley, D. K. Hoang, F. Schlosser, Q. Chen, J. K. Carson, and D. J. Cleland. Transcritical-transcritical cascade CO_2 heat pump cycles for high-temperature heating: A numerical evaluation. *Applied Thermal Engineering*, 238:122005, 2024.

[8] W. Li, S. Kadam, and Z. Yu. Heat transfer enhancement of tubes in various shapes potentially applied to CO_2 heat exchangers in refrigeration systems: Review and assessment. *International Journal of Thermofluids*, 20:100511, 2023.

[9] E. Liang, B. Cheng, C. Zhang, and Y. Yao. Performance analysis and prediction of a modified precompression transcritical CO_2 power generation cycle. *Heliyon*, 10(18):e38108, 2024.

[10] L. Liu, Z. Cao, T. Shen, L. Zhang, and L. Zhang. Experimental and numerical investigation on flow and heat transfer characteristics of a multi-waves internally spiral finned tube. *International Journal of Heat and Mass Transfer*, 172:121104, 2021.

[11] A. Metsue, S. Poncet, and Y. Bartosiewicz. A homogeneous relaxation model algorithm in density-based formulation with novel tabulated method for the modeling of co2 flashing nozzles. *International Journal of Refrigeration*, 161:188–201, 2024.

[12] A. Mota-Babiloni, J. Navarro-Esbrí, A. Barragán-Cervera, F. Molés, B. Peris, and G. Verdú. Commercial refrigeration – an overview of current status. *International Journal of Refrigeration*, 57:186–196, 2015.

[13] Y.-W. Pai and R.-H. Yeh. Experimental investigation of heat transfer and pressure drop characteristics of internal finned tubes. *International Journal of Heat and Mass Transfer*, 183:122183, 2022.

[14] I. Rustum and H. Soliman. Numerical analysis of laminar mixed convection in horizontal internally finned tubes. *International Journal of Heat and Mass Transfer*, 33(7):1485–1496, 1990.

[15] B. Shome. Laminarization of turbulent flow in a heated vertical finned tube. *International Journal of Thermal Sciences*, 159:106597, 2021.

[16] G. Tang, H. Shi, Y. Wu, J. Lu, Z. Li, Q. Liu, and H. Zhang. A variable turbulent prandtl number model for simulating supercritical pressure CO_2 heat transfer. *International Journal of Heat and Mass Transfer*, 102:1082–1092, 2016.

[17] Y. Wang, Q. Zhao, Q. Zhou, Z. Kang, and W. Tao. Experimental and numerical studies on actual flue gas condensation heat transfer in a left–right symmetric internally finned tube. *International Journal of Heat and Mass Transfer*, 64:10–20, 2013.

[18] X. Xu, L. Teng, W. Ran, Y. Wang, and C. Liu. A review of heat transfer deterioration mechanisms and mitigation strategies of supercritical CO_2 heat transfer. *International Journal of Heat and Fluid Flow*, 109:109534, 2024.

[19] N. Zheng, P. Liu, F. Shan, Z. Liu, and W. Liu. Turbulent flow and heat transfer enhancement in a heat exchanger tube fitted with novel discrete inclined grooves. *International Journal of Thermal Sciences*, 111:289–300, 2017.

[20] K. Zolcer Skačanová and M. Battesti. Global market and policy trends for CO_2 in refrigeration. *International Journal of Refrigeration*, 107:98–104, 2019.